ADVANCED OPTICAL MATERIALS
www.advopticalmat.de

Materials Views
www.MaterialsViews.com

Biocompatible and Sustainable Optical Strain Sensors for Large-Area Applications

*Gen Kamita, Bruno Frka-Petesic, Antoine Allard, Marielle Dargaud, Katie King, Ahu Gumrah Dumanli, and Silvia Vignolini**

Plant-based polysaccharides such as cellulose and its derivatives are receiving increasing interest for a large variety of applications because they represent an environmentally friendly alternative to plastics.[1] Many of the cellulose derivatives are commonly used in diverse industrial applications, such as food additives[2] and for biomedical devices[3] due to their nontoxic and water-soluble nature. Moreover, the self-assembly nature[4] and responsiveness[5] of cellulosic biopolymers makes them extremely attractive for smart photonic applications[6,7] including sensing.[8,9] Among various types of cellulose and its derivatives, hydroxypropyl cellulose (HPC) encompasses all these desirable properties, which makes it an extraordinarily multifunctional and versatile material.

Hydroxypropyl cellulose is a liquid crystal polymer, which can form a cholesteric liquid-crystalline phase.[10–12] This liquid crystalline behavior allows Bragg-like reflection of circularly polarized light at specific wavelengths, which is determined by the pitch, the angle of illumination, and the average refractive index of the cholesteric phase.[13,14] Cholesteric liquid crystals are a promising class of responsive optical materials known for their capability to respond to various external stimuli, such as mechanical stress,[15,16] electric field,[17,18] temperature,[18] and light.[15,19] Likewise, the reflected color of HPC can be tuned simply by solvent nature,[14] concentration of the polymer[20] or salt,[21] temperature,[10,14,21] and by applying shear deformation.[22]

In this work, we demonstrate a low-cost method for the fabrication of biocompatible strain-responsive photonic sensors based on an aqueous HPC mesophase. By simply sandwiching the HPC-water mesophase with polymer sheets, we obtain robust, large-area and flexible strain sensors able to detect different types of deformation (e.g., compression, shear, and extension) from the optical signature. The fabricated sensors, therefore, overcome the shortfalls of conventional photonic crystal strain sensors, such as a lack of scalability[23,24] and incompatibility with dry environments[25,26] and conventional electrical strain sensors[27,28] which do not distinguish different deformations. The use of HPC enables synergy between: (i) the optical properties of liquid crystals, (ii) the responsive characteristics of polymers, (iii) the sustainability, biocompatibility, and (iv) abundance of the materials involved. Our results demonstrate that biopolymers can be exploited for responsive large area coatings, which can find use in a wide range of application, including textile, displays, smart fabrics, and also security devices, without compromising scalability and structural integrity.

In order to evaluate the performances of the sensors, we test the optical response as a function of applied strain. An HPC strain sensor before compression is shown in the photograph of **Figure 1**a. When a strain pattern is applied, the pressed region of the sensor shows a vivid blue color (Figure 1b and Video 1 in the Supporting Information). The color shift of the sensor from green to blue is a result of a change in the pitch of the cholesteric structure of HPC (Figure 1c,d), caused by the applied compressive strain. A macroscopic sensor is capable of registering a large and complex pattern, such as handprints (Figure 1e). Diffused reflection spectra measured at different applied strains are shown in Figure 1f. The peaks in the spectra correspond to the colors reflected by the sensor.

The responsive coloration of the developed sensors is a result of the optical properties of the cholesteric liquid crystals. Such a system can be described in first approximation using the de Vries formula for cholesteric liquid crystals[6,29]

$$\lambda = \tilde{n} p \cos\phi \tag{1}$$

where λ is the wavelength at the maximum reflectance (peak wavelength) in vacuum, $\tilde{n} = (n_o + n_e)/2$ is the average refractive index of the liquid crystal, p is the pitch of the cholesteric phase and ϕ is the angle of reflection with respect to the cholesteric helix axis. This equation is valid in the case of infinite cholesteric media with uniaxial orientation of cholesteric axes.

However, in the case of HPC mesophase, the orientation of the cholesteric axis is not uniform throughout a millimeter-thick sample. More specifically, the mesophase consists of cholesteric domains with axes that are randomly tilted by an angle β with respect to the normal of the sample surface. Each of them reflects light specularly with respect to their own axis (**Figure 2**a). From a macroscopic point of view, numerous microreflections occurring at different domains with random tilts appear as a wavelength selective scattering. The angular dependency of such scattering is shown in Figure 2b, where we report the experimentally measured reflectance peak (λ) as a function of the angle θ_{out}. Such a dependence, in the case of low birefringence, can be described by Ferguson's equation[14,30]

Dr. G. Kamita, Dr. B. Frka-Petesic, A. Allard, M. Dargaud, K. King, Dr. A. G. Dumanli, Dr. S. Vignolini
Department of Chemistry
University of Cambridge
Lensfield Road, Cambridge CB2 1EW, UK
E-mail: sv319@cam.ac.uk

The copyright line of this paper was changed 2 November 2016 after initial publiaction.

DOI: 10.1002/adom.201600451

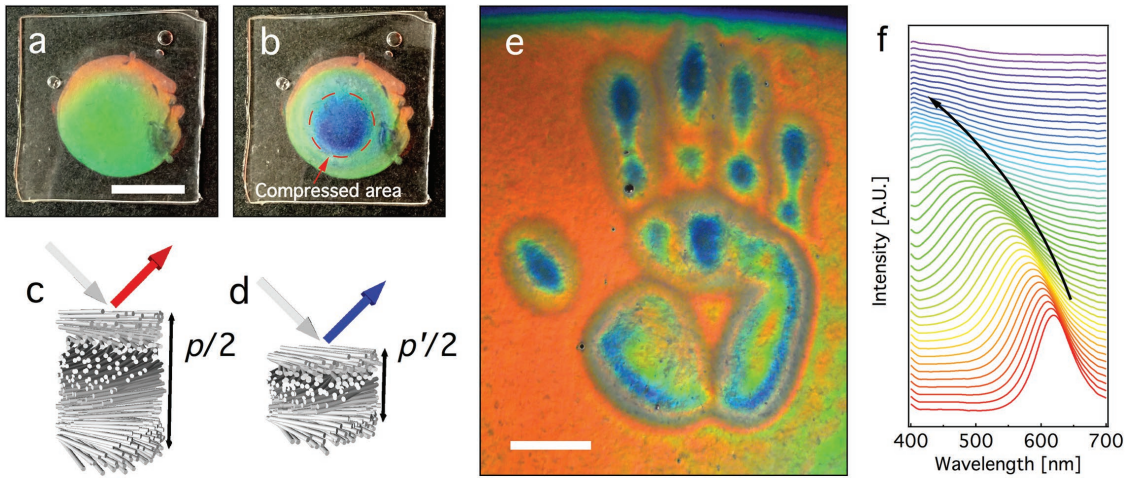

Figure 1. a,b) Photographs of a strain-responsive photonic sensor with PDMS encapsulation a) before and b) after pressing with a solid cylinder. c,d) 3D models of color selective reflection from cholesteric domains. e) A handprint recorded on a macroscopic sensor. f) Spectra of scattered reflection from the strain-responsive photonic sensor. The spectra are incrementally shifted upward for clarity. The arrow indicates the peak shift by increasing strain (2% per step). The measurements were performed at $\theta_{in} = 35°$ and $\theta_{out} = 0°$. The scale bars are 1 cm in (a) and 4 cm in (e).

$$\lambda = \tilde{n} p \cos\left\{\frac{1}{2}\left[\sin^{-1}\left(\frac{1}{\tilde{n}}\sin\theta_{in}\right) + \sin^{-1}\left(\frac{1}{\tilde{n}}\sin\theta_{out}\right)\right]\right\} \quad (2)$$

where θ_{in} and θ_{out} are the angles of the incident and collected light beams.

By assuming p as a constant and using an average optical index of $\tilde{n} = 1.42$ (as calculated from the specific weight and refractive indices of HPC[31,32]), the angular dependency of λ predicted by Equation (3) reproduces the experimental observation, within ±1%. The slight discrepancy can be attributed to the inhomogeneity of the pitch, caused by residual stress that originates from the sample preparation process. Note that the data-points are lacking around $\theta_{out} = 30°$ because the recorded signal is dominated by the specular reflection of the encapsulating material (Figure S1, Supporting Information).

In order to investigate the strain-responsive properties of our system, we perform an angular resolved optical characterization. Scattering spectra of the sensors before and immediately after compression are shown in **Figure 3**a–c as false-color plots. The amount of compression is 0%, 10%, and 15% in (a), (b), and (c) respectively. For all the measurements, θ_{in} is fixed at $\theta_{in} = 0°$, while the scattered signal is collected from different θ_{out}. In all the measurements reported in Figure 3, the peak intensity increases as θ_{out} approaches 0°. This indicates that most of the domains are well aligned and have their helical axis almost perpendicular to the normal of the sample surface. However, the wide range of θ_{out} that allowed detection of peaks, (approximately –50° to 50°) indicates that tilted domains are also present. It is known that HPC mesophase has a pronounced tendency to order at the interface region,[33,34] which implies a localized perpendicular orientation of the helical axis at the surface (anchoring[35]), while being randomly oriented in the bulk.[33,34] Upon compression, the peaks are blue-shifted and broadened accordingly.

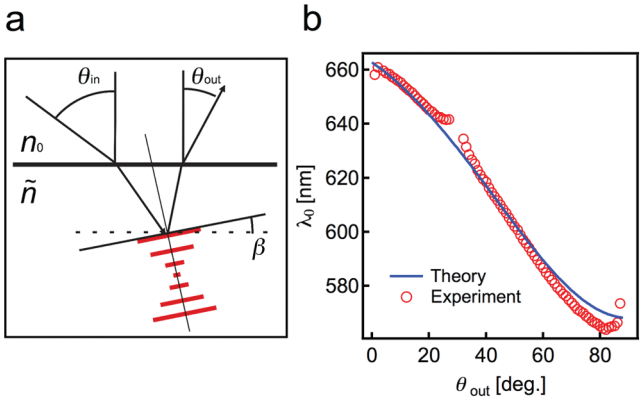

Figure 2. a) Scheme of a ray reflected by a tilted domain illustrating Ferguson's law. b) Peak wavelength plotted with a corresponding theoretical curve according to Ferguson's law.

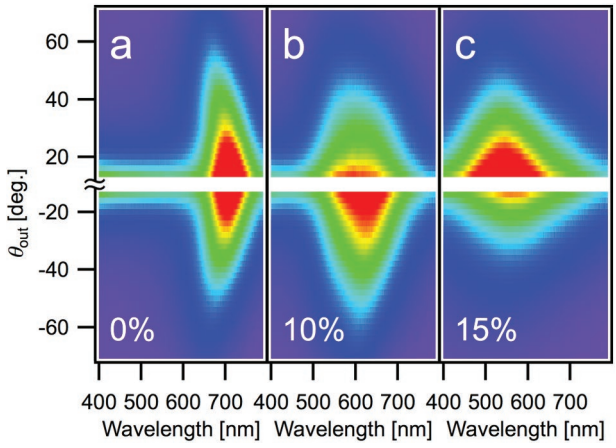

Figure 3. a–c) False-color plots of goniometer scans on HPC mesophase samples, taken with fixed incident angle $\theta_{in} = 0°$. The measurements were taken a) before compression, b) after 10%, and c) 15% of compression. Data from –14° to +14° is left blank because this region was inaccessible due to the mechanical limits of the goniometer.

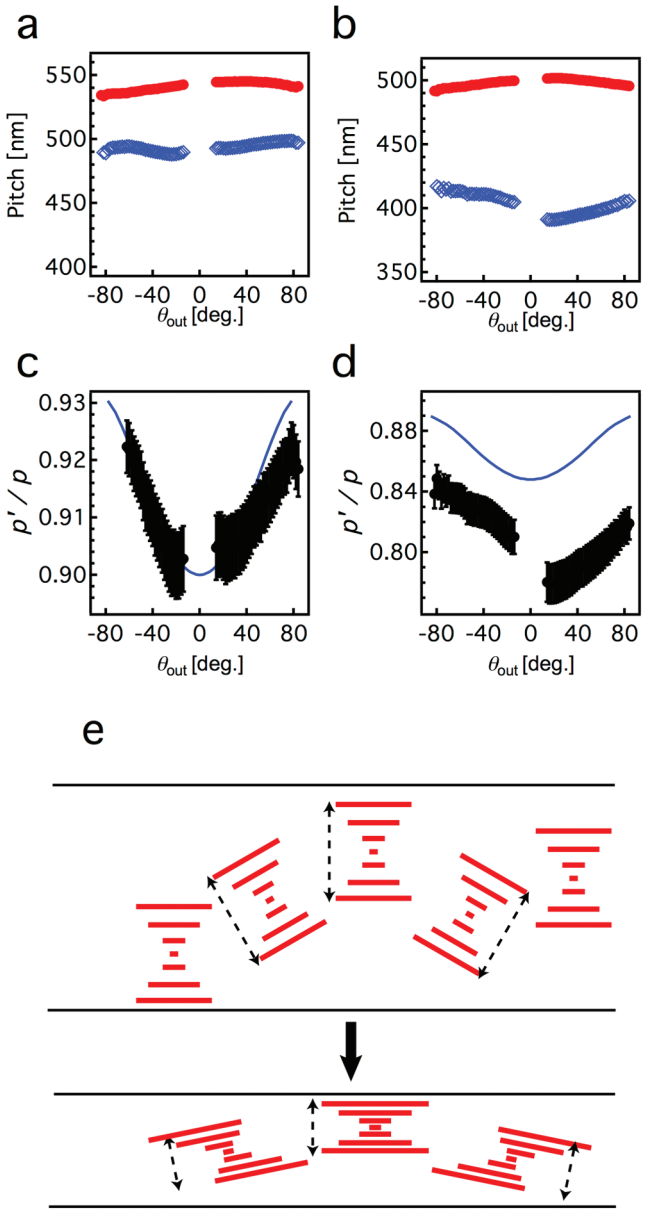

Figure 4. a,b) p (before pressing) and p' (after pressing) plotted as a function of θ_{out}. The measurements were taken with a) 10% and b) 15% compression. c,d) p'/p plotted as a function of θ_{out} for 10% and 15% compression. (e) Illustration of the affine deformation process of the cholesteric domains.

The pitch values of the HPC mesophase extrapolated from Figure 3 using Equation (3) are shown in **Figures 4**a,b, respectively. After 10% compression, the average pitch shift is ≈47 nm, while it increases to 94 nm for a larger compression of 15%. From the measured pitch values, we calculate the ratio of the pitch after and before compression, p'/p, at different θ_{out} as shown in Figure 4c,d, assuming affine deformation of cholesteric domains. The value of p'/p is smaller at lower values of θ_{out}, which can be interpreted as a result of an angle dependent compression of the tilted domains. In other words, both the pitch and the orientation of tilted domains need to be considered in order to describe compressive deformation (Figures S1 and S2, Supporting Information).

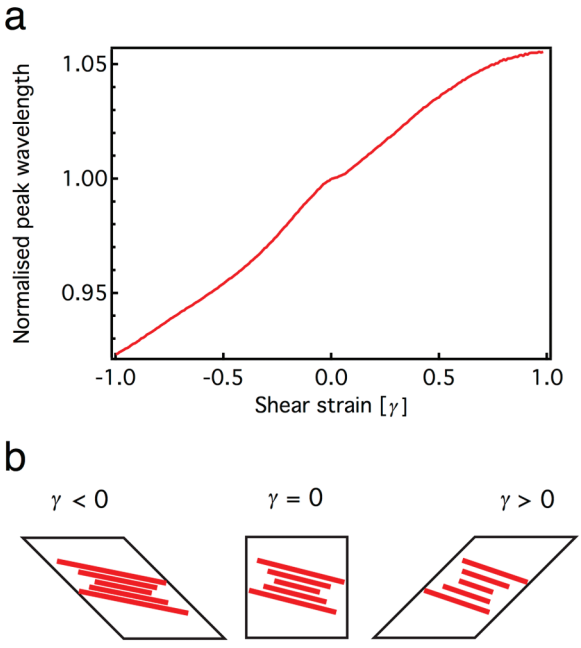

Figure 5. a) Experimentally measured peak shift by shear deformation in opposite directions (positive and negative). The peak wavelength is normalized with respect to its initial state before the shear deformation ($\gamma = 0$). The measurements were performed with fixed angles of $\theta_{in} = 0°$ and $\theta_{out} = 35°$. b) Schematic of the positive and negative shear deformation. A cholesteric domain is illustrated with red lines in order to indicate the detected increase and decrease of the pitch.

The viscoelastic properties of the HPC mesophase are taken into account as an experimental error, which is estimated from the relaxation time measured in a separate optical stress relaxation experiment. In this experiment, two characteristic relaxation times of the peak wavelength value were found, which were 22 min and 3.2 h. Such values are extremely dependent on the concentration and molecular weight. The derivation of the mechanical theory (Figures S1 and S2, Supporting Information) used for the calculation and the results of the optical stress relaxation measurements (Figures S3 and S4, Supporting Information) are provided in the Supporting information. We find that the experimental values in Figure 4c (10% compression) quantitatively agree with the theoretical prediction, supporting our affine deformation theory. With 15% compression, however, the experimental values are significantly lower than the prediction (≈6% mismatch), indicating that the model is predictive for small deformation but becomes less accurate at larger deformations. The quantitative mismatch between theory and experiments at 15% strain can be explained by considering the macroscopic deformation of the HPC mesophase. A detailed discussion of a nonhomogeneous deformation model is reported in the Supporting Information S2.

The orientation-dependent response of the sensor against shear deformation is shown in **Figure 5**. A clear color shift of the sensor is observed when shear deformation is applied (Video 2, Supporting Information). By aligning the plane of incidence with respect to the direction of the shear, it is possible to detect the direction of strain as positive or negative peak shift when the light scattered by tilted domains are measured. When

forward shear ($\gamma > 0$) and backward shear ($\gamma < 0$) are applied to the sensor, red-shift and blue-shift are detected, (Figure 5a) while θ_{in} and θ_{out} are kept constant at 0° and 30°, respectively.

Such color shift therefore depends on the direction of shear and provides insite that can expand the scope of application of our affine deformation model of cholesteric domains; Depending on the orientation of the cholesteric domain with respect to the principal strains, its pitch is not only able to decrease when subjected to strain as described earlyer, but also able to increase as shown schematically in Figure 5b.

Such consideration implies that our model can be robust against different types of deformation. In our model, the relationship between p'/p and β has a unique dependence on the type of the deformation applied (Figure S7, Supporting Information). Therefore, the principal strains and their orientation can be quantified by a simple scattering measurements, allowing the sensors to be used for distinguishing various types of deformation, such as uniaxial strech, compression, shear and anything that comes inbetween.

In conclusion, we successfully demonstrated the fabrication, functionality, and the principle of operation of strain-responsive photonic sensors based on HPC mesophase. The mechanism of the color shift was investigated in detail by studying the sensors under controlled compressive and shear strain. The results of angular-resolved spectroscopy were analyzed with a model that assumes affine deformation, which quantitatively agreed with the experiment at small deformation (up to ≈10%). Using only HPC and water as the active component of the sensor, we are able to detect strain patterns with a direct visible readout with a 2% resolution of strain. Crosslinking of the HPC polymer[36] will allow to further tailor their mechanical behavior. As shown in Figure S8 in the Supporting Information, the HPC sensor responds elastically in a short time scale, with the color change completely reversible upon the removal of strain.

The functionality of these sensors requires HPC to remain in its hydrated state at a known, constant concentration between 60 and 70 wt%—the range that shows an optical response in the visible.[20] Consequentially, the quality of the encapsulation is crucial for the long-term performance of the sensor. As such it is important to note that the large area strain sensor reported here retained its tunable color for over half a year after its fabrication. Only the edges of the sensor, which were exposed to ambient atmosphere without any sealing, locally lost coloration. This observation indicates that, as long as the sensor is large enough, the slow diffusion of water within the film allows the dried HPC to serve as a sealing agent.

The presented results demonstrate that the developed system can be used as a scalable, biocompatible, inexpensive, and renewable stress–strain sensor for biomedical and biomechanical applications, such as for tactile sensors for minimally invasive surgery,[37] foot plantar pressure measurement systems,[38] and motion detection.[39]

Experimental Section

Sample Preparation: HPC was purchased from Sigma-Aldrich (average M_W≈100 kDa) and was used without further purification. An aqueous mesophase of HPC (60 wt%) was prepared by mixing HPC powder and deionized water in centrifuge tubes. The samples were repeatedly mixed with few days intervals between each mix until they attained a homogeneous color. The HPC mesophase was then centrifuged at 48 000 g for 10–15 min. In the next step, three types of strain sensors were prepared.

The first type of strain sensors was prepared by encapsulating the HPC mesophase with polydimethylsiloxane (PDMS). Thin sheets of PDMS were prepared from Sylgard 184. Components A and B of Sylgard 184 were mixed in a ratio of A: B = 10:1 and spread onto microscope slides by airflow from a nitrogen gun. The microscope slides were then placed on a hot plate with a temperature between 40 and 50 °C for a day to cure the PDMS. The cured PDMS sheets were peeled off and cut into square sheets and then place on clean microscope slides. The HPC mesophase was smeared onto the PDMS sheets with a spatula and then spread by pressing it with another PDMS sheet from the top. A fresh mixture of Sylgard 184 was poured onto the sides of the sheets and was allowed to spread between the gaps, making the encapsulation complete. The sensors were placed on a hot plate with a temperature between 40 and 50 °C for a day to cure the PDMS. After the PDMS was cured, the sensors were sonicated in water with a small amount of washing-up liquid. This process promoted detachment of the sensors from the microscope slides. In some experiments, the HPC mesophase were prepared with 0.05 to 0.40 wt% carbon black added to the mixture. The carbon black powder was mixed with the dry HPC powder prior to adding the water and was processed as described previously. The experiments that used carbon black loaded samples are indicated in the main text.

The second type of strain sensor was prepared with microscope slides as encapsulating containers. The HPC mesophase was smeared onto microscope slides with a spatula and were spread by pressing it with clean microscope slides from the top. The thickness of the HPC mesophase was controlled by placing spacers with thicknesses of 0.5–1 mm between the two microscope slides. Prior to the optical measurements, the sensors were allowed to rest for at least a few days in an airtight container, with a damp paper towel included to maintain humidity.

The third type of strain sensor, which was used for recording the handprint, was prepared by spreading the HPC mesophase in an A4 clear file with a spatula. The upper part of the HPC mesophase in the centrifuge tube was used and the bottom part was discarded. The sensor was kept under a glass panel and was left for 3 weeks before experiments.

Optical Characterization: Angular-resolved spectroscopy was carried out using a home-built goniometer.[6,40] A xenon lamp (HPX-2000, Ocean Optics) was used as a light source and a spectrometer (AvaSpec-HS2048, Avantes) was used to extract the scattered optical signal. The sample mounted on the goniometer was illuminated with a slightly focused beam. The light was first collimated using a reflective collimator (RC08SMA-F01, Thorlabs) attached to the optic fiber connected to the light source. The collimated beam was focused on the center of the sample with a planoconvex lens with a focal length of 5 cm. The size of the spot on the sample was ≈1 mm. A detector was mounted on an arm attached to a motorized rotation stage. A reflective collimator mounted on the detector, coupled the scattered light into an optic fiber connected to the spectrometer. The light intensity was normalized with respect to a Lambertian diffuser. In some experiments, the planoconvex lens was removed from the setup and the sample was illuminated by collimated light.

The measurements were performed by either taking a series of measurements by scanning the angle of detection or with fixed angles. In order to capture the state of the sensor immediately after the deformation process, the scans were performed in a short timescale. The goniometer scans were completed within 40 s from the onset of the compression process. The optical properties of strained films display an initial blue shift followed by a long-time relaxation to their original color as the strain is maintained (Figures S2 and S3, Supporting Information). The relaxation time did not depend on the angle β. The spectra were analyzed by fitting them with a Gaussian function and the peak wavelength λ was extracted from the fit curves.

Determination of the Applied Strain: Two methods were employed to determine the compressive strain applied to the HPC mesophase. In the

first method, photographs of the HPC mesophase samples were taken at a fixed distance and their areas were determined by analyzing the photographs with ImageJ. Assuming volumic incompressibility, the stretch ratio of the compressed samples were estimated using the following equation

$$\alpha_1 = \frac{A_{\text{initial}}}{A_{\text{strained}}}, \quad (3)$$

where α_1 is the stretch ratio in the thickness direction of the HPC sample, A_{initial} and A_{strained} are the area of the sample before and after the compression. In the second method, the stretch ratio was calculated from the ratio of the thickness of the HPC mesophase before and after the compression. The thicknesses were measured with a calliper.

Supporting Information

Supporting Information is available from the Wiley Online Library or from the author.

Acknowledgements

This work was supported by the BBSRC David Phillips fellowship [BB/K014617/1], The Isaac Newton Trust Cambridge 76933 and the ERC-2014-STG H2020 639088. The authors thank R. M. Parker and J. Mertens for discussions. All the research data supporting the publication are available from the University of Cambridge data repository (http://dx.doi.org/10.17863/CAM.925).

Received: June 9, 2016
Revised: July 26, 2016
Published online: August 30, 2016

[1] D. Klemm, B. Heublein, H. P. Fink, A. Bohn, *Angew. Chem. Int. Ed.* **2005**, *44*, 3358.
[2] R. A. Kent, R. S. Stephens, J. A. Westland, *Food Technol.* **1991**, *45*, 108.
[3] W. K. Czaja, D. J. Young, M. Kawecki, *Biomacromolecules* **2007**, *8*, 1.
[4] J. H. Park, J. Noh, C. Schütz, G. Salazar-Alvarez, G. Scalia, L. Bergström, J. P. F. Lagerwall, *ChemPhysChem* **2014**, *15*, 1477.
[5] X. Qiu, S. Hu, *Materials* **2013**, *6*, 738.
[6] A. G. Dumanli, G. Kamita, J. Landman, H. van der Kooij, B. J. Glover, J. J. Baumberg, G. Kamita, S. Vignolini, *Prog. Polym. Sci.* **2014**, *2*, 646.
[7] A. G. Dumanli, H. M. van der Kooij, G. Kamita, E. Reisner, J. J. Baumberg, G. Kamita, S. Vignolini, *ACS Appl. Mater. Interfaces* **2014**, *6*, 12302.
[8] M. Giese, L. K. Blusch, M. K. Khan, W. Y. Hamad, M. J. MacLachlan, *Angew. Chem. Int. Ed.* **2014**, *53*, 8880.
[9] Y. P. Zhang, V. P. Chodavarapu, A. G. Kirk, *Sens. Actuators B-Chem.* **2013**, *176*, 692.
[10] G. Charlet, D. G. Gray, *Macromolecules* **1987**, *20*, 33.
[11] R. D. Gilbert, P. A. Patton, *Prog. Polym. Sci.* **1983**, *9*, 115.
[12] D. G. Gray, *J. Appl. Polym. Sci.: Appl. Polym. Symp.* **1983**, *37*, 179.
[13] R. S. Werbowyj, D. G. Gray, *Mol. Cryst. Liq. Cryst.* **1976**, *34*, 97.
[14] R. S. Werbowyj, D. G. Gray, *Macromolecules* **1984**, *17*, 1512.
[15] Q. Li, Y. Li, J. Ma, D.-K. Yang, T. J. White, T. J. Bunning, *Adv. Mater.* **2011**, *23*, 5069.
[16] J. Schmidtke, S. Kniesel, H. Finkelmann, *Macromolecules* **2005**, *38*, 1357.
[17] J. Chen, S. M. Morris, T. D. Wilkinson, H. J. Coles, *Appl. Phys. Lett.* **2007**, *91*, 121118.
[18] L. V. Natarajan, J. M. Wofford, V. P. Tondiglia, R. L. Sutherland, H. Koerner, R. A. Vaia, T. J. Bunning, *J. Appl. Phys.* **2008**, *103*, 093107.
[19] Y. Li, A. Urbas, Q. Li, *J. Am. Chem. Soc.* **2012**, *134*, 9573.
[20] R. S. Werbowyj, D. G. Gray, *Macromolecules* **1980**, *13*, 69.
[21] Y. Nishio, R. Chiba, Y. Miyashita, K. Oshima, T. Miyajima, N. Kimura, H. Suzuki, *Polym. J.* **2002**, *34*, 149.
[22] T. Asada, S. Onogi, *Polym. Eng. Rev.* **1983**, *3*, 323.
[23] A. C. Arsenault, T. J. Clark, G. von Freymann, L. Cademartiri, R. Sapienza, J. Bertolotti, E. Vekris, S. Wong, V. Kitaev, I. Manners, R. Z. Wang, S. John, D. Wiersma, G. A. Ozin, *Nat. Mater.* **2006**, *5*, 179.
[24] H. Fudouzi, T. Sawada, *Langmuir* **2006**, *22*, 1365.
[25] M. A. Haque, G. Kamita, T. Kurokawa, K. Tsujii, J. P. Gong, *Adv. Mater.* **2010**, *22*, 5110.
[26] E. P. Chan, J. J. Walish, E. L. Thomas, C. M. Stafford, *Adv. Mater.* **2011**, *23*, 4702.
[27] H.-U. Ko, S. Mun, S.-K. Min, G.-W. Kim, J. Kim, *Materials* **2014**, *7*, 7000.
[28] W. Wan-Lu, L. Ke-Jun, L. Yong, W. Yong-Tian, *Chin. Phys. Lett.* **2003**, *20*, 1544.
[29] H. de Vries, *Acta Crystallogr.* **1951**, *4*, 219.
[30] J. L. Fergason, *Mol. Cryst.* **1966**, *1*, 293.
[31] Y. Onogi, Y. Nishijima, *Kobunshi Ronbunshu* **1986**, *43*, 223.
[32] Material Safety Data Sheet of Hydroxypropyl Cellulose; MSDS [Online], http://datasheets.scbt.com/sc-252897.pdf (accessed: August 2016).
[33] G. Evmenenko, C. J. Yu, S. Kewalramani, P. Dutta, *Langmuir* **2004**, *20*, 1698.
[34] Y. Onogi, J. L. White, J. F. Fellers, *J. Polym. Sci.: Polym. Phys. Ed.* **1980**, *18*, 663.
[35] B. Jerome, *Rep. Prog. Phys.* **1991**, *54*, 391.
[36] S. N. Bhadani, D. G. Gray, *Mol. Cryst. Liq. Cryst.* **1984**, *102*, 255.
[37] T. Salo, T. Vancura, O. Brand, in *Proc. IEEE Micro Electro Mechanical Systems*, IEEE, Piscataway, NJ, USA **2003**, pp. 590–593.
[38] A. H. Abdul Razak, A. Zayegh, R. K. Begg, Y. Wahab, *Sensors* **2012**, *12*, 9884.
[39] T. Yamada, Y. Hayamizu, Y. Yamamoto, Y. Yomogida, A. Izadi-Najafabadi, D. N. Futaba, K. Hata, *Nat. Nanotechnol.* **2011**, *6*, 296.
[40] S. Vignolini, E. Moyroud, B. J. Glover, U. Steinera, *J. R. Soc. Interface* **2013**, *10*, 20130394.